Journal of Power Sources 219 (2012) 36–44

Contents lists available at SciVerse ScienceDirect

Journal of Power Sources

journal homepage: www.elsevier.com/locate/jpowsour

Enhanced thermal safety and high power performance of carbon-coated $LiFePO_4$ olivine cathode for Li-ion batteries

K. Zaghib [a,*], J. Dubé [a], A. Dallaire [a], K. Galoustov [a], A. Guerfi [a], M. Ramanathan [b], A. Benmayza [b], J. Prakash [b,**], A. Mauger [c], C.M. Julien [d]

[a] Institut de Recherche d'Hydro-Quebec, 1800 Boul. Lionel Boulet, Varennes, QC, Canada J3X
[b] Center for Electrochemical Science and Engineering, Department of Chemical and Biological Engineering, Illinois Institute of Technology, Chicago, IL 60616, USA
[c] Université Pierre et Marie Curie-Pari6, Institut de Minéralogie et de Physique des Milieux Condensés (IMPMC), 4, Place Jussieu, 75252 Paris Cedex 05, France
[d] Université Pierre et Marie Curie-Pari6, Laboratoire de Physicochimie des Electrolytes, Colloïdes et Sciences Analytiques (PECSA), 4, Place Jussieu, 75252 Paris Cedex 05, France

HIGHLIGHTS

- Safety of C–$LiFePO_4$, $LiNi_{0.8}Co_{0.15}Al_{0.05}O_2$, $LiNi_{0.33}Co_{0.33}Mn_{0.33}O_2$ and $LiCoO_2$ are reported.
- Crush, nail penetration, short circuit tests are reported in video and discussed.
- Ni and Al doping did not improve the thermal stability of the lamellar compounds.

ARTICLE INFO

Article history:
Received 26 March 2012
Received in revised form
7 May 2012
Accepted 10 May 2012
Available online 2 July 2012

Keywords:
$LiFePO_4$
Olivine oxide cathode
Li-ion cells
Thermal runaway
Thermal safety

ABSTRACT

The carbon-coated $LiFePO_4$ Li-ion oxide cathode was studied for its electrochemical, thermal, and safety performance. This electrode exhibited a reversible capacity corresponding to more than 89% of the theoretical capacity when cycled between 2.5 and 4.0 V. Cylindrical 18,650 cells with carbon-coated $LiFePO_4$ also showed good capacity retention at higher discharge rates up to 5C rate with 99.3% coulombic efficiency, implying that the carbon coating improves the electronic conductivity. Hybrid Pulse Power Characterization (HPPC) test performed on $LiFePO_4$ 18,650 cell indicated the suitability of this carbon-coated $LiFePO_4$ for high power HEV applications. The heat generation during charge and discharge at 0.5C rate, studied using an Isothermal Microcalorimeter (IMC), indicated cell temperature is maintained in near ambient conditions in the absence of external cooling. Thermal studies were also investigated by Differential Scanning Calorimeter (DSC) and Accelerating Rate Calorimeter (ARC), which showed that $LiFePO_4$ is safer, upon thermal and electrochemical abuse, than the commonly used lithium metal oxide cathodes with layered and spinel structures. Safety tests, such as nail penetration and crush test, were performed on $LiFePO_4$ and $LiCoO_2$ cathode based cells, to investigate on the safety hazards of the cells upon severe physical abuse and damage.

1. Introduction

Lithium-ion batteries have dominated the battery industry for the past several years in portable electronic devices due to their high volumetric and gravimetric energy densities. It was expected that the success of these batteries in small scale applications would translate to large scale applications, which would have an important impact in the future of the environment by improving energy efficiency and reducing pollution. Safety of lithium-ion rechargeable batteries has been the technical obstacle for high power demand applications [1]. Lithium ion batteries under normal usage are generally safe. However, safety of Li-ion battery under abusive conditions is still a technical barrier for applications such as hybrid electric vehicles (HEV) and electric vehicles (EV), and the safety too often relies on the battery monitoring system (BMS). This thermal runaway is not only a safety hazard but also hinders the performance of lithium ion batteries eventually.

Even though the mechanism of thermal runaway is initiated by the anode in combination with the electrolyte [2], the rapid temperature rise in the cell, which dominates the overall heat generated during this process, is produced by the cathode reacting

* Corresponding author. Tel.: +1 450 652 8019; fax: +1 450 652 8424.
** Corresponding author.
E-mail addresses: zaghib.karim@ireq.ca (K. Zaghib), prakash@iit.edu (J. Prakash).

0378-7753/$ – see front matter © 2012 Elsevier B.V. All rights reserved.
http://dx.doi.org/10.1016/j.jpowsour.2012.05.018

with the electrolyte [3,4]. Therefore, it is of utmost importance to find a more structurally stable cathode in order to use lithium batteries at their fullest potential [5].

Lithium ion cells have historically used lithium metal oxides as cathode materials due to their high capacity for lithium intercalation, and suitable chemical and physical properties required for Li-ion electrodes. Layered materials with $LiMO_2$ structure, where M = Co, Ni, Mn, or a combination of these metals, have been the most extensively used and investigated cathodes. These types of cathodes show excellent performance, but suffer from higher cost, toxicity ($LiCoO_2$), and thermal instability ($LiNiO_2$). In order to avoid these problems, another lithium metal oxide material with spinel structure $LiMn_2O_4$ has been proposed to substitute the layered materials. This oxide is inexpensive and environmentally friendly, but has disadvantages related to capacity fade issues, especially at high temperatures. Recently, an olivine structure material ($LiFePO_4$) has emerged as a possible cathode replacement, and abundant focus of research [6–12] on $LiFePO_4$ in the past and in recent years has been made owing to its desirable properties such as (1) relatively inexpensive material cost, (2) high average cycling voltage due to flat potential of 3.4 V *vs.* Li/Li^+, (3) reasonably high theoretical capacity 170 mAh g^{-1}, (4) relatively less toxic compared to $LiCoO_2$ systems, and (5) most of all, ability to suppress thermal runaway to make the Li-ion battery thermally safe. This property is attributed to the high covalent feature of the P–O bonds in the tetrahedral (PO_4) units, which stabilizes the olivine structure and prevents oxygen release from the charged (delithiated) olivine materials up to 600 °C [13,14]. This is still controversial in other members of the olivine family $LiMPO_4$. In particular, a thermal instability has been reported in the charged (i.e. delithiated) state of $LiMnPO_4$ and $LiCoPO_4$ [15–18]. However, in a recent study, the LiFePO4 and LiMnPO4 cathode materials were found to have comparable thermal stability in their pristine and fully delithiated states [19]. On another hand, there is an overall agreement on the remarkable thermal stability of $liFePO_4$ and its delithiated counterpart [15,16], and the recognition that $LiFePO_4$ is a safer cathode material than the commonly used lithium metal oxide cathodes with layered structures [3,20,21].

Nevertheless, $LiFePO_4$ material suffers from poor electronic conductivity [22]. This leads to poor rate capability that has limited the use of $LiFePO_4$ for high power density HEV and EV applications. Hence, a conductive carbon coating on the surface of $LiFePO_4$ was introduced to enhance the conductivity of the electrode and tailor $LiFePO_4$ electrode more suitable to high power density HEV and EV applications [8–12,24–26]. This paper will discuss the improvement in electrochemical and thermal properties of Lithium iron phosphate ($LiFePO_4$) protected with a thin layer of carbon as a cathode material.

2. Experiments and methods

2.1. Coin cell fabrication

$LiFePO_4$/Li and graphite/Li half-cells were prepared using a carbon-coated $LiFePO_4$ electrode and graphite anode supplied by Hydro-Quebec, Canada. The scanning electron microscope (SEM) image in Fig. 1. shows that the average size of the carbon-coated $LiFePO_4$ particles is 150 nm. The positive electrode contained 89% $LiFePO_4$ particles 150 nm in diameter coated with carbon as active cathode material, 3% vapor grown carbon fiber, 3% carbon acetylene black (CAB) and 5% PVDF binder and metallic lithium foil was used as negative electrode. The electrodes were dried at 120 °C under a vacuum and then transferred to argon filled glove box. The coin cells were 20 mm in diameter and 3.2 mm thick (2032 coin cells). A Celgard (3501) surfactant coated porous polypropylene separator,

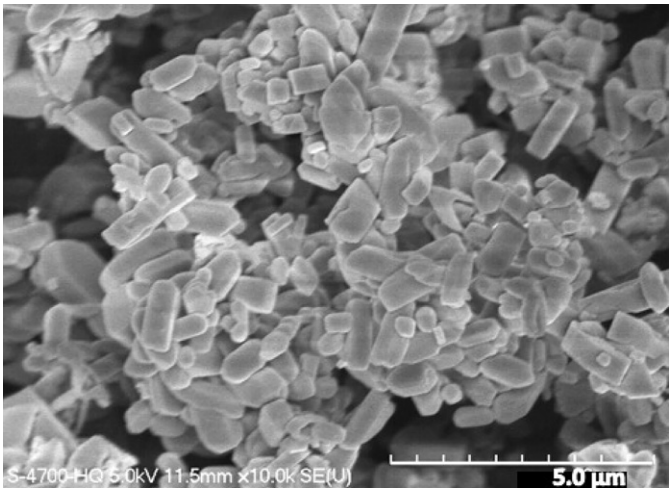

Fig. 1. SEM image of the C–$LiFePO_4$ particles used as the active cathode element of the $LiFePO_4$//Li coin cells and the $LiFePO_4$//C 18,650 cells in the present work.

1.2 mol L^{-1} $LiPF_6$ in ethylene carbonate (EC) and ethyl methyl carbonate (EMC) (wt% 3:7) electrolyte, and lithium metal foil were also used within the stainless steel case to fabricate 2032 size coin cell. All cells were assembled in an argon-filled glove box and galvanostatically cycled at 0.1C rate from 2.5 to 4 V five times at constant temperature of 25 °C in a BT-2043 Arbin cycler. The graphite anode laminate was composed of carbon-coated graphite, VGCF, and binder. The anode half-cell preparation also went through the same process as the cathode half-cell. The cells were cycled 5 times at constant temperature of 25 °C at rate of 0.1C from 1 to 10^{-3} V in BT-2043 Arbin cycler. Fully delithiated cathode material from coin cells was used to measure thermal stability of cathode using Differential Scanning Calorimeter (DSC). Coin cells using spinel ($LiMn_2O_4$) and layered ($LiNi_{0.8}Co_{0.15}Al_{0.05}O_2$) oxides synthesized at IIT, were also prepared to compare thermal stability of different cathode chemistries.

2.2. Differential scanning calorimetry

The thermal stability of the $LiFePO_4$ cathode, along with other cathode materials and anode material was studied using differential scanning calorimetry (DSC-Perkin-Elmer Pyris 1 differential scanning calorimeter). After cycling the cells five times at 0.1C rate and obtaining the proper capacity, the cells were fully-charged and subsequently subjected to 8 h of trickle charge at constant voltage of 4.2 V to ensure the cathode material is completely delithiated. Then, they were introduced into the dry glove box. The cells were opened carefully and the cathode material was recovered. The electrodes were slightly dried and then scratched to obtain the cathode material. 3–6 mg of active material samples from each electrode were packed into small stainless steel DSC capsules and then hermetically sealed. The samples were scanned in the DSC equipment under nitrogen purging from 50 to 400 °C at a 10 °C min^{-1} heating rate.

2.3. Experiments on commercial 18,650 cells

Hydro-Quebec (HQ), Canada, supplied the cylindrical 18,650-size cells consisting of carbon-coated LiFePO4 as the cathode material and the carbon-coated graphite as the anode material. The laminate composition in the 18,650-cell was the same as used in the coin cell mentioned in Section 2.1. The thermal properties of HQ cylindrical 18,650 size cells of 1.4 Ah capacity were investigated

under various states of charge and discharge using an isothermal calorimeter (IMC). The thermal runaway behavior of the same cell at fully charged state was investigated using an accelerating rate calorimeter (ARC). The dynamic power capabilities of carbon-coated $LiFePO_4$//graphite based commercial 18,650 size cells, supplied by Hydro-Quebec were studied with a Hybrid pulse power characterization (HPPC) test [27].

2.3.1. Hybrid Pulse Power Characterization

One of the applications where Li-ion batteries are considered as an immediate solution is in large-scale applications where high power is required. HPPC test emulates the requirements of cells used in HEVs and PHEVs on the road. HPPC test was performed on fully charged cell by applying sequence of pulse containing discharge 10% of capacity, followed by 1 h rest, 3C discharge pulse for 18 s, 32 s rest, and series of regenerative charging pulses for 10 s. The next pulse begins again after 10 s rest and discharge again 10% capacity of the cell. The scheme of the HPPC profile is illustrated in Fig. 2. The HPPC test profile was developed to study the useable power and voltage range of cells at different depths of discharge (DOD).

2.3.2. Isothermal microcalorimetry

The isothermal microcalorimeter (IMC, Model CSC 4400, Calorimetry Science Corp.) was used to measure the rate of heat released/absorbed by the 18,650 cell during charge/discharge process, monitored simultaneously in a BT-2043 Arbin cycler. The cell chamber temperature of the IMC was controlled to be at 25 °C. The difference in the heat flow rate between the sample cylindrical cell and the reference cylindrical cell was recorded as the output heat flow rate from cell reactions. To examine the effect of discharge rate on the heat flow rate, the 18,650 cell was cycled at different discharge rates (0.1C, 0.2C, and 0.5C). Two hours of rest was maintained between every charge and discharge to recover the residual heat completely from the cell. This relaxation period ensures prevention of mixing of charge and discharge heats.

2.3.3. Accelerating rate calorimeter

Accelerating Rate Calorimeter (Arthur D. Little ARC2000) was used to measure the thermal stability of the commercial cylindrical 18,650-size cell. The 18,650 cell was fully charged to 4.0 V, followed by 24 h of trickle charge at constant voltage of 4.0 V and subsequently transferred to ARC. The ARC setup consists of three heaters, top, base and side heaters, each equipped with individual thermocouples to ensure uniform heating across the entire chamber and thus the cell is heated uniformly as well. The ARC was operated based on Heat-Wait-Search (HWS) mode which consists of heating the cell from 40 to 450 °C at a heating rate of 5 °C min^{-1} in the heating mode for every 10 °C step. The waiting mode allows the temperature to equilibrate for 20 min and then ARC searches for an exothermal heat release from the cell (>0.02 °C min^{-1}) for 15 min during the search mode. If the calorimeter detects self-heat rate greater than or equal to 0.02 °C min^{-1}, it will track that exothermic heat released by the cell reactions, otherwise the temperature is stepped up by 10 °C for the next HWS mode. Thus the HWS mode continues until the cell undergoes thermal decomposition (sample-to-chamber temperature difference>100 °C) is detected or the final temperature (450 °C) is reached.

2.3.4. Safety tests

Video of nail penetration, which was performed to investigate the safety behavior of a cell under penetration of a strong nail into the cell, is shown in the results section of this article. Prior to the test, the cell was fully-charged at a rate of C/6. Once the desired state of charge was reached, the cell was carefully placed and safely fastened on to a specially designed stand. The thermocouple was placed behind the cell, which makes it not visible in the attached video. During the nail penetration test, the cell was perforated with nail and the position of the nail was maintained inside the cell for the entire duration of the experiment. The voltage, current, and temperature of the cell were measured over time to assess the damage induced during and after nail penetration. For the crush test, the cell was crushed to approximately 50% of its thickness. Both the nail penetration and crush test were performed in a way to emulate enforced internal short-circuit of the cell. After the test, the cell was allowed to cool in ambient conditions for a minimum of 1 h so that the temperature drops and no further reaction occurs. The experiments were performed in a closed room specifically designed for destructive tests. The room was ventilated after the tests to evacuate any gases that were liberated during the experiment.

3. Results and discussion

Fig. 3 shows the electrochemical performance of the carbon-coated $LiFePO_4$ in a half-cell for the first seven charge/discharge cycles at C/10 rate. The behavior clearly indicates a single long

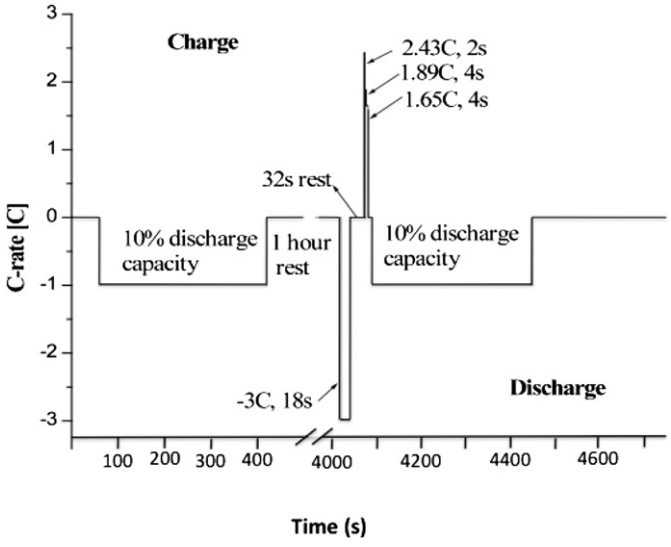

Fig. 2. Hybrid Pulse Power Characterization (HPPC) profile [27] for cylindrical 18,650 cells.

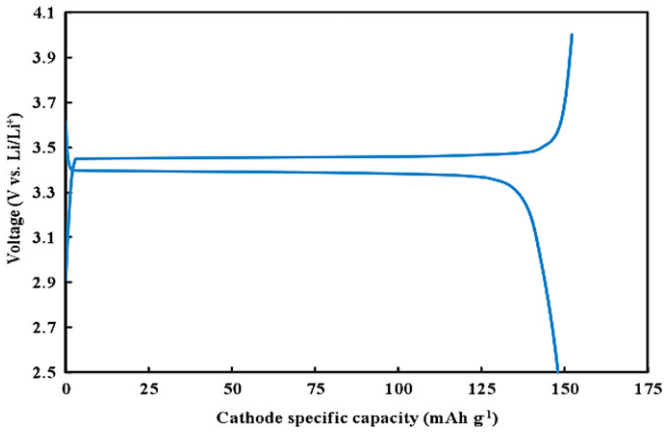

Fig. 3. Electrochemical performance of initial seven 0.1C rate charge/discharge cycles for carbon-coated $LiFePO_4$/Li 2032 coin cell (the curves of the seven cycles are superposed).

plateau around 3.4 V *vs.* Li/Li$^+$. Carbon-coated $LiFePO_4$ exhibited more than 97% coulombic efficiency and a consistent reversible discharge capacity ~ 152 mAh g^{-1}, which is more than 89% of its theoretical capacity, when cycled between 2.5 and 4.0 V. This capacity is in agreement with our prior works [28]. It is, however, significantly smaller than the theoretical value close to 170 mAh g^{-1} because the tests were performed on a 2032 coin cell, and we have already reported that the capacity in such cells is systematically smaller by about 10 mAh g^{-1} lower than the value measured in 18,650 cells with the same powder [29]. It can be seen that the carbon-coated $LiFePO_4$ electrode exhibited a discharge voltage plateau at 3.43 V *vs.* Li/Li$^+$ corresponding to the two-phase $LiFePO_4/FePO_4$ transformation [12]. These results are an improvement of the performance of uncoated $LiFePO_4$ electrodes [12,23,30,31] and some carbon-coated electrodes [24] found in literature.

Fig. 4 shows the rate capability of the carbon-coated $LiFePO_4$// graphite cylindrical 18,650 cell at 0.1C, 0.2C, 0.5C, 1C, 2C, and 5C rates. The same cycling rates during charge and discharge were used for all measurements and the cells were cycled in the same potential window as used in coin cells. The cell had consistently high reversible discharge capacity of 1.42 Ah when discharged at 0.1C rate. These cylindrical cells also showed very good capacity retention when cycled at 0.1C rate and only 1.3% capacity loss was observed after 70 cycles of charge and discharge at 0.1C rate. The coulombic efficiencies obtained at all the different charge/discharge rates exceeded 99.3%. Fig. 5 shows the discharge capacity of C–$LiFePO_4$//graphite 18,650-size cell at various cycling rates and for multiple cycles. It can be seen that the cell maintained similar discharge capacities when cycled at rates slower than 1C-rate, and the cell was able to retain 90% of the initial capacity for rates up to 5C rate. These results just illustrate that carbon-coated active material exhibited higher capacity retention at higher discharge currents, compared with non-coated particles [32,33]. Most importantly, the cell regained the 1.42 Ah capacity when the cell was cycled at the initial 0.1C charge and discharge rate. The loss of capacity at high discharge rates is attributed to the increase in the internal resistance and is followed by full capacity recovery. Post rate capability tests indicated that the cathode material did not undergo any degradation during high discharge rates.

A cylindrical 18,650 cell using carbon-coated HQ $LiFePO_4$ as positive electrode was subjected to HPPC test after 70 cycles at 0.1C rate, and then cycled again up to 100 cycles at 0.1C rate, after which one more HPPC test was performed on the 18,650 size cylindrical cell. Fig. 6 illustrates the applied current and measured voltage profile after the cylindrical cells were cycled up to 70 and 100 cycles. Even after 70 cycles of charge and discharge, the HQ cell was able to withstand 9 high-rate discharge and regenerative charge pulses and the cell was able to withstand 8 high-rate pulses after 100 cycles.

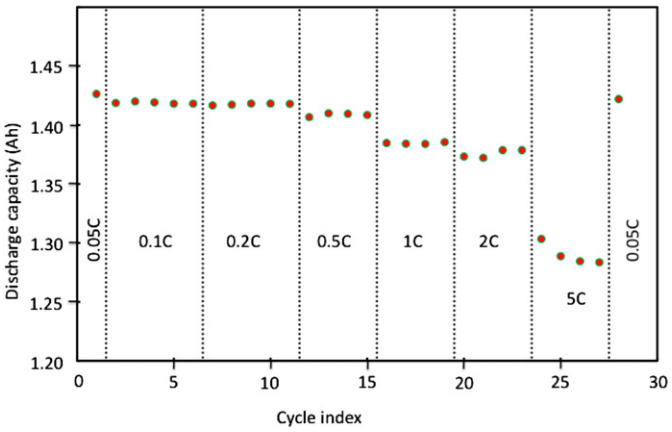

Fig. 5. Discharge capacity of C–$LiFePO_4$//graphite 18,650 cell for different C-rates to illustrate capacity retention at higher C-rates.

This cell was able to deliver 3.2 V down to 80% DOD and the calculated cell resistances ($\Delta V/\Delta I$) at different SOC indicated that cell resistance remained lower than 34.3 mΩ to 80% DOD for both 18 s discharge pulses and 10 s regenerative charge pulses. Again cell resistance of discharge pulses were consistently higher than that of regenerative charge pulse and the values ranged between 14 and 34 mΩ only. The difference between the resistance of charge and discharge is due to the HPPC procedure reported in Fig. 1: the discharge is a continuous process while the charge is pulsed regime. This cell also showed consistent pulse power capacity as evident from very low differential discharge pulse power drop and regenerative pulse power gain, which is illustrated in Fig. 7. Average power values indicated that 80% of discharge power can be applied back to the cell in the form of regenerative charging on this cell. Again no significant change in resistances and pulse power capacity were observed in both 18 s discharge pulse (DP) and 10 s regenerative charge pulse (RGP) down to 80% depth of discharge (DOD) for cell tested after 70 and 100 cycles. HPPC results indicated that carbon-coated $LiFePO_4$ electrodes are very well suited for HEV applications. The performance of $LiFePO_4$ electrodes at high

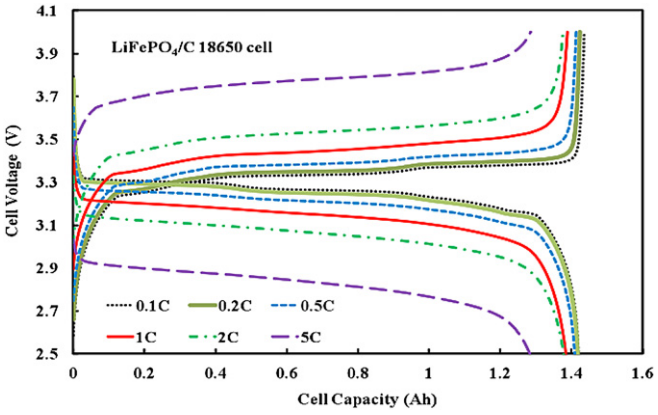

Fig. 4. Rate capability result on C–$LiFePO_4$//graphite 18,650 cell at different discharge rates. The different plateaus at low C-rates correspond to the different phases of Li_xC_6 on the negative electrode.

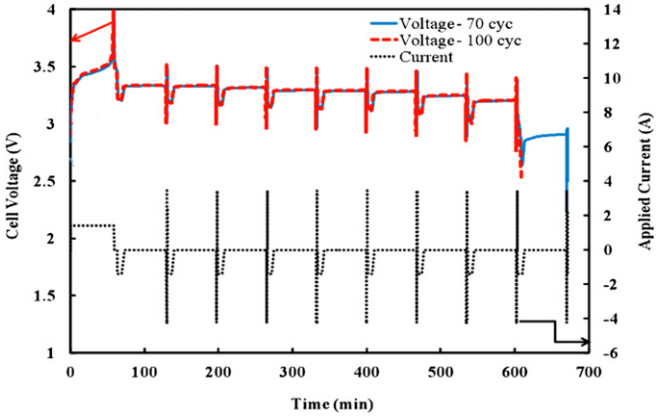

Fig. 6. HPPC results for a C–$LiFePO_4$//graphite 18,650 cell after 70 and 100 cycles of charge/discharge at 0.1C rate. The results after 70 cycles and 100 cycles cannot be distinguished, and the two voltage–time profiles are superposed.

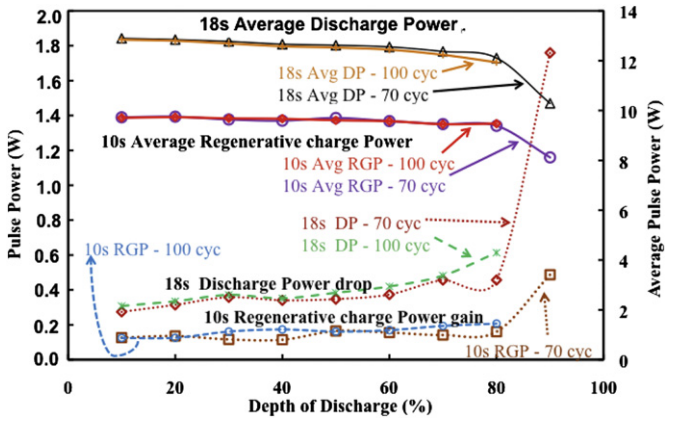

Fig. 7. Differential pulse power drop/gain (left scale) and pulse power capacity (right scale) of the C–$LiFePO_4$//graphite 18,650 cell at different states of charge. The symbols are experimental results under the conditions defined as ns (duration in number of seconds) of the discharge pulse (DP) or regenerating charge pulse (RGP) after 70 and 100 cycles (cyc).

discharge rates and the high power of the 18,650 cell were attributed mainly to the electronic conductivity improvement achieved through carbon-coating of the positive electrode.

Fig. 8 shows the generated heat rate and the voltage profiles of a cylindrical 18,650 size cell at different rates (0.1C, 0.2C, and 0.5C) at 25 °C. 2 h rest period of time was left between each charge and discharge, so that there is no overlap between charge-discharge heats. These profiles were reproducible for up to 3 cycles for each rate. It can be seen from the figure that the overall exothermic heat generated during charge and discharge process increased with respect to the C-rate. This overall heat released from the cylindrical 18,650-size cell includes the reversible heat due to the entropic change of the cell reaction, and the irreversible heat due to the deviation of the cell potential from its equilibrium potential [34]. Table 1 shows the accumulated exothermic heat values obtained by the calculation of the area under the heat rate profile during the charge/discharge process. The cell relaxation heat released during the 2 h rest period between every charge and discharge was also included in the estimation of accumulated heat during charge/discharge.

At low C-rate, the generated heat during discharge process was increased by 90% from 0.1C to 0.2C. This heat, at low C-rates, includes the nearly balanced contribution of both the reversible

Table 1
Accumulated heat released and the estimated cell temperature rise during charge/discharge of the cylindrical 18,650 size C–$LiFePO_4$//graphite cell at different C-rate.

C-rate	Accumulated heat (J)		Estimated ΔT (°C)	
	Charge	Discharge	Charge	Discharge
C/10	216	197	2.9	2.6
C/5	420	375	5.6	5.0
C/2	689	645	9.3	8.5

entropic and irreversible resistive heat, as the heat rate profiles show non-monotonous behavior which is attributed to the sign changes of entropy values [35] occurring during charge/discharge. However, at higher rate, 0.5C, the generated heat was increased by 227%, and this was mainly due to the dominance of the irreversible resistive heat over the reversible entropic heat, because of the significant increase of the overpotential caused by the enormous rise in the ohmic resistance and also the electrodes polarization as a result of conversion to $FePO_4$ phase [34]. This conversion is achieved at 3.6 V *vs.* Li^+/Li, and $FePO_4$ is known to be very resistive acting as a limiting current element. The delithiated material does not generate exothermic reaction because of the absence of Li ions [36]. Nevertheless, the heat generated at 0.5C rate remains very moderate, and actually too small to cause any thermal runaway.

The estimated cell temperature showed rise of 9.3 °C during charge and 8.5 °C during discharge at 0.5C rate, which indicates the cell temperature at the surface will reach 34 °C when no external cooling is applied during charge/discharge. The cell surface temperatures were estimated using cell average heat capacity value of 75 J g^{-1} reported elsewhere [37] and the integrated heat values. The estimated cell temperatures at the surface were found to be less than SEI decomposition temperature and hence carbon-coated $LiFePO_4$ is considered to be a safe material that retains its reversible chemical structure during the continuous charge and discharge processes.

Fig. 9 illustrates the DSC spectra of the fully delithiated and over charged carbon-coated $LiFePO_4$ and the spectra of the fully lithiated carbon-coated graphite, both electrodes with traces of 1.2 mol L^{-1} $LiPF_6$ in EC-EMC (3:7), measured at a scan rate of 10 °C min^{-1} from 50 to 400 °C. The traces of electrolyte in the samples prepared for DSC were calculated to be between 15 and 20% weight of the electrode tested. The onset temperature of the lithiated anode and delithiated cathode was detected at 80 and 245 °C respectively. By convention, we note with a negative sign the heat that is lost by the

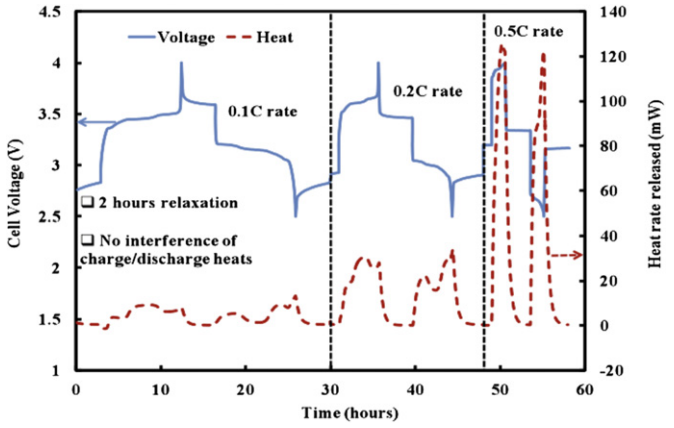

Fig. 8. Generated heat rate (broken curve, right scale) and voltage profiles (full curve left scale) of a cylindrical 18,650 size C–$LiFePO_4$//graphite cell during cycling using an isothermal microcalorimeter.

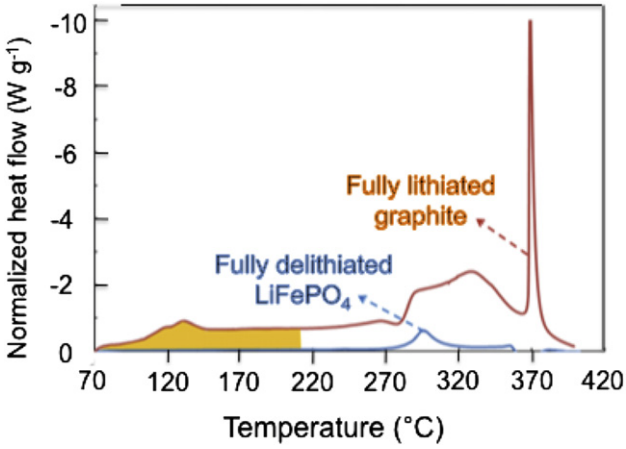

Fig. 9. DSC spectra of fully lithiated graphite and over charged $LiFePO_4$ with traces of 1.2 mol L^{-1} $LiPF_6$ in EC-EMC (3:7) electrolyte at 10 °C min^{-1}.

system under consideration, i.e. a negative peak in the figure means an exothermic peak. The variation of enthalpy is reported in Table 2. In particular, the heat generated from the lithiated graphite was −170 J g^{-1} for temperatures between 67 and 200 °C, which corresponds to the SEI layer decomposition interval; this heat represents the contribution of the lithiated graphite to initiate the overall thermal runaway in a full cell. Enthalpy of anode reaction beyond 200 °C was not included, as most of the cathode chemistries start degrading at this temperature. However, the delithiated cathode, the most responsible electrode in the thermal runaway, showed very good stability under the DSC test. The calculated enthalpy of cathode reaction in the range of 50–400 °C was −250 J g^{-1} and this heat is a result of higher oxidation state of Fe occurring in fully charged cathode, which undergoes exothermic reaction with the electrolyte. These results are in good agreement with early studies [38] and indicate a significant improvement in the thermal properties of $LiFePO_4$ cathode compared to the commonly used lithium metal oxide layered materials [39]. This result proved that the lithium iron phosphate is distinguished material cathode in term of safety due to the strong P–O covalent bonds in $(PO_4)^{3-}$ polyanion, which prohibits the oxygen liberation [40]. Delayed reaction onset temperature and considerably smaller reaction enthalpy for $LiFePO_4$ cathode is mainly attributed to high activation energy needed to break the strong P–O bond for oxygen release. It can also be seen that reaction enthalpy of cathode was found to be lesser than that of graphite anode and any effects of the combination can be observed in ARC measurements discussed later in this article.

Fig. 10 shows DSC spectra of the over charged spinel ($LiMn_2O_4$), layered ($LiNi_{0.8}Co_{0.15}Al_{0.05}O_2$) cathode and carbon-coated $LiFePO_4$, all electrodes with traces of 1.2 mol L^{-1} $LiPF_6$ in EC-EMC (3:7), measured at a scan rate of 10 °C min^{-1} from 50 to 400 °C. We can observe that both spinel and olivine cathodes have delayed onset temperature by at least 70 °C with respect to the layered cathode. The layered cathode was found to be thermally unsafe, as this cathode undergoes its exothermic reaction with very large enthalpy (−941 J g^{-1}) and the reaction gets completed at much earlier temperature, lower than the onset temperature of spinel and olivine. Spinel cathode showed roughly half the exothermic reaction enthalpy (−439 J g^{-1}), whereas carbon-coated olivine showed even lesser exothermic reaction enthalpy (−250 J g^{-1}). The results are summarized in Table 2.

Based on their previous experimental results, Prakash et al. [39] proposed that a possible mechanism leading to the thermal runaway of the layered cathode consists of the following four steps:

Step 1**:** The first step involves a partial structural deformation of $Li_xNi_{0.8}Co_{0.15}Al_{0.05}O_2$ into disorder oxide (spinel-like structure) and liberation of small amount of oxygen from it as a result of this structural deformation.

Step 2**:** This step entails the reaction of the oxygen produced in step-1 with the ethylene carbonate due to its lower flash point of 150 °C:

Table 2
Flow of enthalpy deduced from the DSC spectra of the fully delithiated and over charged carbon-coated $LiFePO_4$ and the fully lithiated carbon-coated graphite (see Fig. 8); that of the over charged cathode elements investigated (see Fig. 9) are reported in the three last columns.

Cell	Range of T (°C)	ΔH (J g^{-1})
$LiFePO_4$//graphite	250°C ≤ T ≤ 360 °C	−96.6
Graphite//Li	250°C ≤ T ≤ 360 °C	−170
Cathode material	Onset T (°C)	Overall ΔH (J g^{-1})
$LiNi_{0.8}Co_{0.15}Al_{0.05}O_2$	170	−941
$LiMn_2O_4$	264	−439
$LiFePO_4$	245	−250

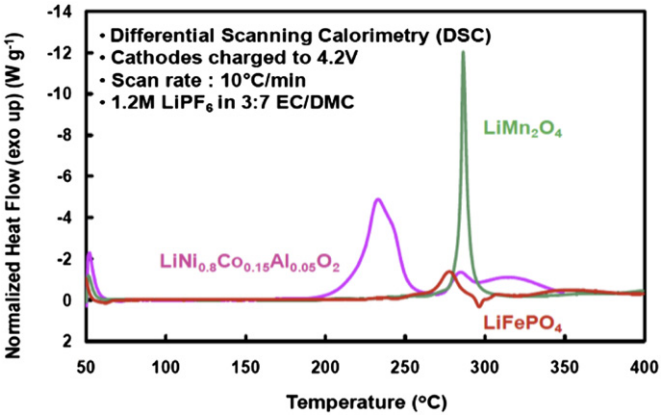

Fig. 10. DSC spectra of over charged layered, spinel and olivine cathodes with traces of 1.2 mol L^{-1} $LiPF_6$ in EC-EMC (3:7) electrolyte at 10 °C min^{-1}.

$$C_3H_4O_3 + 2.5O_2 \rightarrow 3CO_2 + 2H_2O. \quad (1)$$

The continuous reaction of the oxygen with EC and possibly EMC releases combustion heat in the system and raises the temperature.

Step 3**:** The heat released in the above reaction further accelerates the structural deformation, which finally leads to complete structural collapse of the oxide:

$$Li_{0.36}Ni_{0.8}CO_{0.15}Al_{0.05}O_2 \rightarrow 0.18Li_2O + 0.8NiO + 0.05Co_3O_4 + 0.025Al_2O_3 + 0.372O_2. \quad (2)$$

Step 4**:** The large amount of oxygen and heat produced in the above reaction helps the combustion of the remaining electrolyte (EC, EMC, and $LiPF_6$) to produce thermal runaway.

$$C_3H_4O_3 + 2.5O_2 \rightarrow 3CO_2 + 2H_2O, \quad (3)$$

$$C_3H_8O_3 + 2.5O_2 \rightarrow 3CO_2 + 2H_2O. \quad (4)$$

However, in $LiFePO_4$, phase transformation to $FePO_4$ is considered to occur in step 1 rather than structure disordering observed in layered cathode. Step 2 is observed to the same extent found in layered cathode, whereas step 3 is mostly prevented as the heat released from combustion of the solvents with O_2 is used to maintain the $FePO_4$ phase, hence the structural stability of the $LiFePO_4/FePO_4$ cathode. Again, the strong P–O covalent bonds in $(PO_4)^{3-}$ polyanion found in $LiFePO_4$ significantly reduce the rate of O_2 release, thereby reducing the combustion step itself and causing no further damage to the cathode structure.

It was observed in IMC results on $LiFePO_4$ that the cell temperature is raised to not more than 34 °C during charge and discharge at 0.5C rate, and DSC measurements showed that $LiFePO_4$ is less reactive with electrolyte at high temperatures than spinel and layered cathodes. Moreover fully lithiated graphite was observed to show more exothermic heat than $LiFePO_4$ cathode itself, resulting from SEI layer decomposition. So a fully charged cylindrical 18,650 cell using $LiFePO_4$/graphite was tested in Accelerating Rate Calorimeter (ARC) to realize the overall combination of exothermic reaction heats of $LiFePO_4$, graphite and electrolyte. The simultaneous cell temperature and heater temperature and in-situ cell open-circuit potential recorded during ARC test of the cell is reported in Fig. 11. It shows that the cell was heated uniformly as the thermocouples placed in top, side and base of the heater indicated the same temperature during the course of the

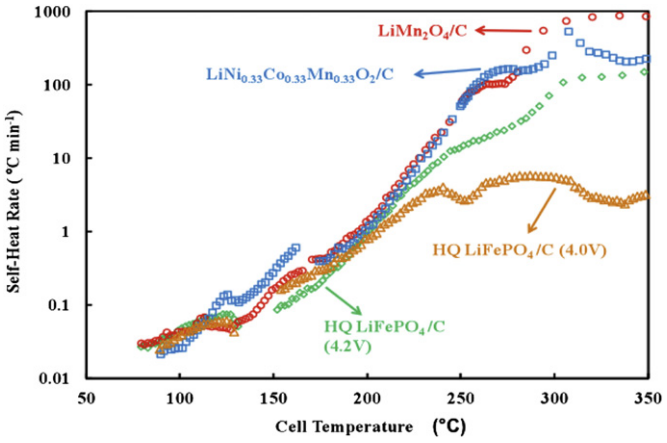

Fig. 11. Cell temperature measured at side, top and base of the heater (the curves are superposed) and in-situ open-circuit potential chronological record of $LiFePO_4$/C 18,650 cell subjected to ARC test.

experiment, and the cell temperature also closely followed the heater temperature until any self-heat was released from the cell. Open-circuit potential remained constant around 3.3 V during this period. At temperature about 80 °C after 160 min from the start of the experiment, the cell started to show self-heat at a rate greater than 0.02 °C min^{-1}. Once the self-heat is released from the cell and is sustained for more than 30 min, the heater begins to follow the cell temperature to the same rate of self-heat. Open-circuit potential also began to gradually drop due to the resistive heating of the cell. After 1455 min of testing, the cell temperature began to rise sharply at a temperature of 150 °C and open-circuit potential began to drop rapidly. This behavior of the cell was attributed to internal short-circuit of the cell owing to the melting of the separator. At 1756 min of test, the cell completely decomposed and the cell temperature completely shot off from that of the heater temperature by more than 80 °C; the cell voltage abruptly fell close to zero in few minutes later.

Fig. 12 shows the self-heat rate (SHR) released from the 18,650 cell ($LiFePO_4$//graphite) fully charged to 1.42 Ah capacity, when heated up to 450 °C in ARC. The figure illustrates three different exothermic reactions. The first self-heat exotherm was observed between 90 and 130 °C, and it is mainly attributed to the reaction of the carbonaceous material in combination with the electrolyte

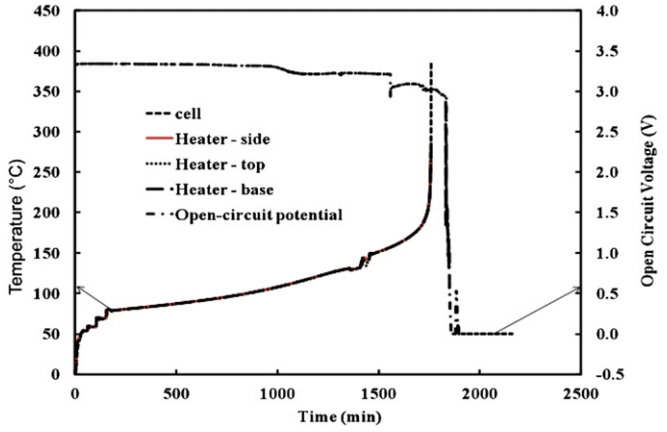

Fig. 12. Self-heat rates of fully-charged 18,650 cells with spinel, layered and olivine cathodes measured in ARC. Self-heat rates of olivine cathode over charged to 4.2 V are also shown.

caused by the SEI layer decomposition [40]. At temperatures above 150 °C, which corresponds to the melting temperature of the separator, the second self-heat exotherm was initiated, causing the cathode to be exposed to reaction with electrolyte. Cathode was subsequently decomposed at temperatures larger than 245 °C and reacted with the electrolyte, releasing more heat and increasing the cell temperature further up. At temperatures above 260 °C, the oxygen released from the composed cathode reacted with the organic solvents, initiating the third self-heat exotherm that corresponds to the beginning of the thermal runaway. However, the cell remained safe and did not explode for temperatures up to 450 °C, since the maximum self-heat rate of the cell was found to be less than 6 °C min^{-1} only. It is deduced that the peak producing the maximum self-heat rate of 6 °C per minute at 286 °C corresponds to the major exothermic reaction as described in the DSC study. The SHR observed in the ARC study of $LiFePO_4$ cathode was significantly lower than the layered oxide and spinel cathodes, indicating the thermal stability of the olivine cathode. The onset temperature and maximum SHR for different cathode chemistries are listed in Table 3. It is observed that even an over charged (to 4.2 V) LiFePO4/C cell showed only 158 °C min^{-1} maximum SHR, compared to 532 and 878 °C min^{-1} maximum SHR observed in layered and spinel oxide cathodes.

DSC results indicated higher exothermic reaction enthalpy for layered oxide than spinel cathode, but the maximum SHR of spinel was found to be higher than that of the layered oxide. On the other hand, the maximum SHR temperature in ARC and the exothermic reaction peak temperature in DSC were found to be consistent. To study this inconsistency of reaction enthalpy and maximum SHR, a DSC experiment was performed for fully-delithiated cathode, $Li_{0.36}Ni_{0.8}Al_{0.05}O_2$, in the presence and absence of the electrolyte. Fig. 13 shows the DSC traces of $Li_xNi_{0.8}Co_{0.15}Al_{0.05}O_2$ in the presence and absence of electrolyte (1.2 mol L^{-1} $LiPF_6$ in EC-EMC (3:7)). One major exothermic reaction is detected at 225 °C, followed by complex small peaks. The major exothermic peak (−731 J g^{-1}), starting at 204 °C and reaching a maximum at 224 °C, is attributed to the structural change of the delithiated cathode accompanying the oxygen liberation and combustion of the electrolyte with the liberated oxygen [39]. The following multiple peaks are attributed to the reaction of the remaining electrolyte with the continuous decomposition of the cathode. A decrease in the heating rate of the rinsed sample as shown in Fig. 13 suggests that the major exothermic reaction at about 225 °C is due to the reaction of the delithiated cathode and the electrolyte.

Hence it is clear that the layered cathode material reacts prematurely with the electrolyte and in the process does not have enough electrolyte to react further. This behavior is consistent with the maximum SHR observed for layered oxide at a much earlier temperature 307 °C than spinel, and the SHR was not sustained after the complete exhaustion of electrolyte at 307 °C. Hence, the $LiFePO_4$ cell exhibited excellent safety, much better than other chemistries, considering the facts that they have very large onset temperature and very low self-rate to remotely cause any thermal runaway of the Li-ion cell.

Table 3
Comparison of accelerating rate calorimeter parameters for the different chemistries (anode in graphite): T_{Onset} is the temperature at the onset of self-heat rate (SHR), the next column is the maximum value of the SHR, which occurs at the temperature given in the last column.

Cathode	T_{Onset}, °C	Max SHR, °C min	$T_{Max\ SHR}$, °C
$LiNi_{0.8}Co_{0.15}Al_{0.05}O_2$//C	74	532	307
$LiMn_2O_4$//C	79	878	334
$LiFePO_4$//C (4.0 V)	89	6.1	286
$LiFePO_4$//C (4.2 V)	89	158	353

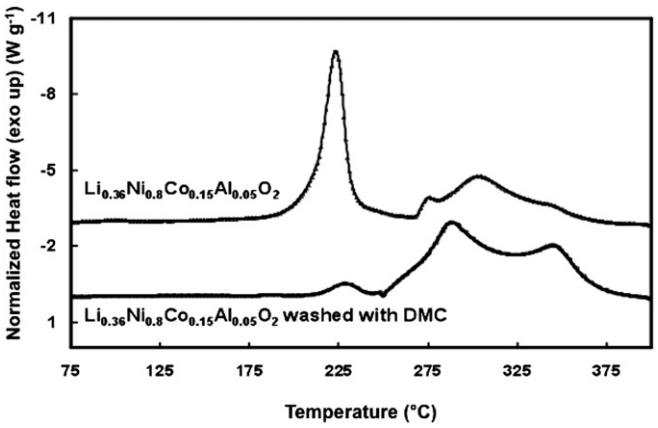

Fig. 13. DSC traces of $Li_xNi_{0.8}Co_{0.15}Al_{0.05}O_2$ in the presence and absence of electrolyte (1.2 mol L^{-1} $LiPF_6$ in EC-EMC (3:7)).

Safety tests were performed for $LiCoO_2$ and carbon-coated $LiFePO_4$ based 18,650 cells in their fully charged state. The resulting videos of the crush and nail penetration tests are provided in the supplementary information. Before the crush test, the cell was charged to 3.7 V and the cell temperature was 26 °C. For the cell with $LiCoO_2$ cathode, the crush test resulted in immediate spark and lot of smoke, causing the cell temperature to increase from 27 to 352 °C in 14 s and the cell voltage dropped from 4.46 to 0 V in few seconds (see Video-1 in Supplementary information). On the other hand, the crush test for the cell with olivine oxide cathode produced a maximum temperature of 98 °C in 24 s with cell voltage still showing 0.05 V for carbon-coated $LiFePO_4$ cell (see Video-2 in Supplementary information). Nail penetration on cells fabricated with $LiCoO_2$ cathode showed immediate spark and smoke, causing the cell temperature to increase from 27 to 352 °C in 14 s and the cell voltage dropped from 4.46 to 0 V in few seconds (see Video-3 in Supplementary information). The nail penetration test on cells fabricated with $LiFePO_4$ cathode revealed that the cell reached a maximum temperature of 103 °C, with a small amount of electrolyte escaping from the cell. For both the tests on $LiFePO_4$ cell, no smoke, no flame, and no explosion were observed (see Video-4 in Supplementary information). The thermal studies carried out on Li_xCoO_2 show that the delithiated $LiCoO_2$ decomposes to CoO or Co_2O_3 and releases O_2 at about 240 °C [41,42]. As a result, an extensive amount of heat is produced when the remaining electrolyte reacts with the released O_2 [41–44]. The DSC results in Fig. 12 show very similar trend as observed in other studies for $LiNiO_2$ [41–43]. In spite of the doping of the present cathode with cobalt and aluminum, it seems that the thermal stability of $LiNi_{0.8}Co_{0.15}Al_{0.05}O_2$ has similar reaction mechanisms to Li_xNiO_2. On the other hand, the strong nature of P–O bond in $(PO_4)^{3-}$ polyanion results in less rate of O_2 release and thus prevents $LiFePO_4$ cell from thermal runaway, unlike in the case of $LiCoO_2$.

Supplementary video related to this article can be found at http://dx.doi.org/10.1016/j.jpowsour.2012.05.018.

4. Conclusion

The carbon-coated $LiFePO_4$ showed excellent electrochemical performance reaching 152 mAh g^{-1}. This electrode also exhibited a reversible capacity corresponding to more than 89% of the theoretical capacity when cycled between 2.5 and 4.0 V. Cylindrical 18,650 cells with carbon-coated $LiFePO_4$ showed only 1.3% discharge capacity loss for 100 cycles at 0.1C rate and also delivered 90% of capacity retention at higher discharge rates up to 5C rate with 99.3% coulombic efficiency, implying that the carbon coating improves the electronic conductivity. Low cell resistances and 80% recovery of discharge pulse power through regenerative charge pulse during HPPC test performed on $LiFePO_4$ 18,650 cell indicated the suitability of this carbon-coated $LiFePO_4$ for high power HEV applications. The heat generation during charge and discharge at 0.5C rate, studied using IMC, indicated that the cell temperature is not raised above 34 °C in absence of external cooling. Thermal studies were also investigated by DSC and ARC, which showed that $LiFePO_4$ is safer, upon thermal and electrochemical abuse, than the commonly used lithium metal oxide cathodes with layered and spinel structures. Video of safety tests performed on $LiFePO_4$ cathode based cells, indicated that $LiFePO_4$ cells withstand physical abuse without causing any safety hazard, whereas $LiCoO_2$ causes instantaneous fire and smoke upon safety tests. In addition, the investigation of $LiNi_{0.8}Co_{0.15}Al_{0.05}O_2$ has revealed that the introduction of Ni and Al as the doping element did not improve the thermal stability, which is then a recurrent problem in layered compounds. The dissolution of manganese in the electrolyte of $LiMn_2O_4$ spinel//graphite cells has been the motivation to add to the spinel a layer compound acting as a trap of manganese, in order to decrease the capacity fade. The present work, however, shows that it amounts to introduce in the cells an unstable element with very poor thermal stability. Therefore, delivery of high power and safety upon thermal, electrochemical and physical abuse makes carbon-coated $LiFePO_4$ more suitable for HEV applications.

References

[1] H. Joachin, T.D. Kaun, K. Zaghib, J. Prakash, ECS Transactions 6-25 (2008) 11.
[2] H.J. Bang, H. Yang, K. Amine, J. Prakash, J. Electrochem. Soc. 152 (2005) A73.
[3] H. Joachin, T.D. Kaun, K. Zaghib, J. Prakash, J. Electrochem. Soc. 156 (2009) A401.
[4] Chang Woo Lee, Rajeev Venkatachalapathy, J. Prakash, Electrochem. Solid-State Lett. 3 (2000) 63.
[5] D.D. Mac Neil, Z. Lu, Z. Chen, J.R. Dahn, J. Power Sources 108 (2002) 8.
[6] J. Li, T. Suzuki, K. Naga, Y. Ohzawa, T. Nakajima, Mater. Sci. Eng. B 142 (2007) 86.
[7] M. Takahashi, H. Otsuka, K. Akuto, Y. Sakurai, J. Electrochem. Soc. 152 (2005) A899.
[8] M. Yonemura, A. Yamada, Y. Takei, N. Sonoyama, R. Kanno, J. Electrochem. Soc. 151 (2004) A1352.
[9] K. Zaghib, J. Shim, A. Guerfi, P. Charest, K.A. Striebel, Electrochem. Solid-State Lett. 8 (2005) A207.
[10] I. Belharouak, C. Johnson, K. Amine, Electrochem. Commun. 7 (2005) 983.
[11] J. Jiang, J.R. Dahn, Electrochem. Commun. 6 (2004) 39.
[12] A.K. Padhi, K.S. Nanjundaswamy, C. Masquelier, J.B. Goodenough, J. Electrochem. Soc. 144 (1997) 2581.
[13] A. Yamada, S.C. Chung, K. Hinokuma, J. Electrochem. Soc. 148 (2001) A224.
[14] M. Armand, J.-M. Tarascon, Nature 451 (2008) 652.
[15] G. Chen, T.J. Richardson, J. Power Sources 195 (2010) 1221.
[16] G. Chen, T.J. Richardson, J. Electrochem. Soc. 156 (2009) A756.
[17] S.-W. Kim, J. Kim, H. Gwon, K. Kang, J. Electrochem. Soc. 156 (2009) A635.
[18] N.N. Bramnik, K. Nikolowski, D.M. Trots, H. Ehrenberg, Electrochem. Solid-State Lett. 11 (2008) A89.
[19] S.K. Martha, O. Haik, E. Zinigrad, I. Exnar, T. Drezen, J.H. Miners, D. Aurbach, J. Electrochem. Soc. 158 (2011) A1115.
[20] S.K. Martha, B. Markovsky, J. Grinblat, Y. Gofer, O. Haik, E. Zinigrad, D. Aurbach, T. Drezen, D. Wang, G. Deghenghi, I. Exnar, J. Electrochem. Soc. 156 (2009) A541.
[21] S.K. Martha, J. Grinblat, O. Haik, E. Zinigrad, T. Drezen, J.H. Miners, I. Exnar, A. Kay, B. Markovsky, D. Aurbach, Angew. Chem. Int. Ed. 48 (2009) 8559.
[22] M. Konarova, I. Taniguchi, Pow. Tech. 191 (2009) 111.
[23] T. Nakamura, Y. Miwa, M. Tabuchi, Y. Yamada, J. Electrochem. Soc. 153 (2006) A1108.
[24] S. Yang, Y. Song, P.Y. Zavalij, M.S. Whittingham, Electrochem. Commun. 4 (2002) 239.
[25] N. Ravet, Y. Chouinard, J.F. Magnan, S. Besner, M. Gauthier, M.J. Armand, J. Power Sources 97 (2001) 503.
[26] K. Zaghib, A. Mauger, M. Kopec, F. Gendron, C.M. Julien, ECS Transactions 16-42 (2009) 31.
[27] Q. Wu, W. Lu, J. Prakash, J. Power Sources 88 (2000) 237.
[28] M.L. Trudeau, D. Laul, R. Veillette, A.M. Serventi, A. Mauger, C.M. Julien, K. Zaghib, J. Power Sources 196 (2011) 7383.
[29] K. Zaghib, M. Dontigny, A. Guerfi, P. Charest, I. Rodrigues, A. Mauger, C.M. Julien, J. Power Sources 196 (2011) 3949.
[30] H.C. Shin, W.I. Cho, H. Jang, J. Power Sources 159 (2006) 1383.

[31] F. Gao, Z. Tang, Electrochim. Acta 53 (2008) 5071.
[32] K. Zaghib, P. Charest, M. Dontigny, A. Guerfi, M. Lagacé, A. Mauger, M. Kopek, C.M. Julien, J. Power Sources 195 (2010) 8280.
[33] C.M. Julien, A. Mauger, K. Zaghib, J. Mater. Chem. 21 (2011) 9955.
[34] H. Yang, J. Prakash, J. Electrochem. Soc. 151 (2004) A1222.
[35] W. Lu, H. Yang, J. Prakash, Electrochim. Acta 51 (2006) 1322.
[36] J.F. Whitacre, K. Zaghib, W.C. West, B.V. Ratnakumar, J. Power Sources 177 (32008) 528.
[37] C. Forgez, D.V. Do, G. Friedrich, M. Morcrette, C. Delacourt, J. Power Sources 195 (2010) 2961.
[38] E.M. Jin, B. Jin, D.K. Jun, K.H. Park, H.B. Gu, K.W. Kim, J. Power Sources 178 (2008) 801.
[39] H.J. Bang, H. Joachin, H. Yang, K. Amine, J. Prakash, J. Electrochem. Soc. 153 (2006) A731.
[40] K. Dokko, S. Koizumi, K. Sharaishi, K. Kanamura, J. Power Sources 165 (2007) 656.
[41] J.R. Dahn, E.W. Fuller, M. Obrovac, U. von Sacken, Solid State Ionics 69 (1994) 265.
[42] D.D. McNeil, J. R Dahn, J. Electrochem. Soc. 148 (2001) A1205.
[43] K.K. Lee, W.S. Yoon, K.B. Kim, K.Y. Lee, S.T. Hong, J. Electrochem. Soc. 148 (2001) A716.
[44] Y. Baba, S. Okada, J.I. Yamaki, Solid State Ionics 148 (2002) 311.